Characterization of Leukemic Resistance to CD19-Targeted CAR T-cell Therapy through Deep Genomic Sequencing

Gregory M. Chen[1], Chia-Hui Chen[2], Jessica Perazzelli[2], Stephan A. Grupp[2,3], David M. Barrett[2,3], and Kai Tan[1,2,3]

ABSTRACT

Chimeric antigen receptor (CAR) T-cell therapy targeting CD19 has been a clinical breakthrough for pediatric B-cell acute lymphoblastic leukemia (B-ALL), and loss of the CD19 target antigen on leukemic cells represents a major mechanism of relapse. Previous studies have observed *CD19* mutations specific to CD19$^-$ relapses, and we sought to clarify and strengthen this relationship using deep whole-exome sequencing in leukemic cells expanded in a patient-derived xenograft. By assessing pretreatment and relapse cells from 13 patients treated with CAR T-cell therapy, 8 of whom developed CD19$^-$ relapse and 5 of whom developed CD19$^+$ relapse, we demonstrate that relapse-specific single-nucleotide variants and small indels with high allele frequency combined with deletions in the *CD19* gene in a manner specific to those patients with CD19$^-$ relapse. Before CAR T-cell infusion, one patient was found to harbor a preexisting *CD19* deletion in the context of genomic instability, which likely represented the first hit leading to the patient's subsequent CD19$^-$ relapse. Across patients, preexisting mutations and genomic instability were not significant predictors of subsequent CD19$^-$ relapse across patients, with sample size as a potential limiting factor. Together, our results clarify and strengthen the relationship between genomic events and CD19$^-$ relapse, demonstrating this intriguing mechanism of resistance to a targeted cancer immunotherapy.

Introduction

Chimeric antigen receptor (CAR) T-cell therapy targeting CD19 has been reported to have overall remission rates as high as 82% in pediatric B-cell acute lymphoblastic leukemia (B-ALL), yet relapses are common, with approximately 41% of patients with initial responses relapsing within 12 months (1). A major mechanism of relapse to CD19-targeted CAR T-cell therapy appears to be the selective expansion of CD19$^-$ leukemic clones, an intriguing mechanism of therapy resistance that was reported in the early trials (2) and has been subsequently shown to likely represent the majority of relapses (1). Genomic sequencing of CD19$^-$ relapses has suggested that somatic mutations within the coding regions of the *CD19* gene are the main mechanism behind the CD19$^-$ cell surface phenotype. Sotillo and colleagues (3) report coding mutations, such as frameshift and missense mutations, in 3 out of 4 CD19$^-$ relapse cases, and Orlando and colleagues (4) subsequently observed coding mutations in 12 out of 12 CD19$^-$ relapse cases. Alternative splicing of exon 2 is suggested as a mechanism of partial rescue of CD19 function in cells with coding mutations in the *CD19* gene (3), although there is little evidence that this represents an independent mechanism of antigen escape from somatic mutations, and alternative splicing was observed at very low frequencies in the cohort of Orlando and colleagues (4).

We hypothesized that deep (>400X) whole-exome sequencing (WES) would allow for accurate and high-confidence detection of somatic mutations and allow for assessment of exome-wide mutational burden. Furthermore, we hypothesized that the assessment of patients with CD19$^+$ relapse would serve as a control to further understand the background rates of *CD19* mutations in B-ALL and strengthen the association between *CD19* mutations and CD19$^-$ relapse.

Materials and Methods

Patient identification, clinical annotation, and sample preparation

Patients were identified by the clinical practices at the Children's Hospital of Philadelphia Division of Oncology (Philadelphia, PA). Patients were enrolled onto Children's Hospital of Philadelphia Institutional Review Board–approved clinical trials NCT01626495 and NCT02906371, with written informed consent obtained by patients or their guardians in accordance with the U.S. Common Rule. Inclusion criteria included patients with B-ALL treated on trial with CD19-targeted CAR T-cell therapy. Exclusion criteria included patients with a malignancy other than B-ALL or patients for whom CAR T-cell infusion was not performed. CAR T-cell treatment was performed as described previously in the clinical protocols. Leukemic cells were isolated from either peripheral blood or bone marrow. We used a Ficoll technique (GE, cat# 17–1440–02) to isolate the peripheral blood mononuclear cells. The patient sample was overlayed on top of a Ficoll layer in a 15-mL conical tube, centrifuged at 2,000 rpm for 15 minutes at room temperature (centrifuge brake off). The buffy coat was then removed, washed with PBS, and counted. Sample information can be found in Supplementary Table S1.

[1]Graduate Group in Genomics and Computational Biology, University of Pennsylvania, Philadelphia, Pennsylvania. [2]Center for Childhood Cancer Research, The Children's Hospital of Philadelphia, Philadelphia, Pennsylvania. [3]Department of Pediatrics, University of Pennsylvania, Philadelphia, Pennsylvania.

Current address for D.M. Barrett: Tmunity Therapeutics, Inc., Philadelphia, PA.

Corresponding Author: Kai Tan, University of Pennsylvania, 3501 Civic Center Boulevard, Philadelphia, PA 19104. Phone: 267-425-0050; E-mail: tank1@chop.edu

Cancer Immunol Res 2023;11:13–9

doi: 10.1158/2326-6066.CIR-22-0095

Patient-derived xenograft expansion of leukemic cells and WES

All experiments using mice were performed in accordance with and with the approval of the Institutional Animal Care and Use Committee at Children's Hospital of Philadelphia. Leukemic cells from 13 patients at preinfusion and relapse time points were engrafted into an NSG patient-derived xenograft (PDX) mouse model as previously described (5), with 7,000 to 20 million cells initially engrafted and engraftment over 4 to 12 weeks. First-passage or second-passage mice were sacrificed when they expressed some combination of the following human surface markers via flow cytometry using a BD FACS Verse: CD10 (BD Biosciences #555375), CD19 (BD Biosciences #555412), CD22 (BD Biosciences #562860), CD34 (Invitrogen #46–0349–42), and/or CD45 (BD Biosciences #560367). Spleens containing engrafted human leukemic cells were harvested and cryopreserved. Mouse cells were negatively selected by flow cytometry sorting with a mouse (m)CD45$^-$ gate (clone: 40-F11, BioLegend #103107), and human cells were positively selected by sorting for human (h)CD45$^+$ (clone: HI30, BD Biosciences #555485) or hCD19$^+$ (clone: FMC63, Sigma #MAB1794H). The sorting was performed on a BD FACSAria Fusion sorter. Genomic DNA was purified using the QIAGEN ALLPrep DNA/RNA Mini kit (QIAGEN #80204), and whole-exome capture and genomic sequencing was performed by GENEWIZ (South Plainfield) using the Twist Human Exome Kit and Illumina HiSeq using the 2×150 bp sequencing configuration.

Per the GENEWIZ protocol, genomic DNA was quantified using Qubit 2.0 Fluorometer (Thermo Fisher Scientific). Enrichment probes were designed against the region of interest and synthesized through Twist Biosciences—Twist Human Comprehensive Panel (South San Francisco, CA), with library preparation performed according to the manufacturer's guidelines. Genomic DNA was fragmented by acoustic shearing with a Covaris S220 instrument. Fragmented DNAs were cleaned up and end repaired, as well as adenylated at the 3′ends. Adapters were ligated to the DNA fragments, and adapter-ligated DNA fragments were enriched with limited cycle PCR. Adapter-ligated DNA fragments were validated using Agilent TapeStation (Agilent Technologies) and quantified using Qubit 2.0 Fluorometer. Adapter-ligated DNA fragments were hybridized with biotinylated baits. The hybrid DNAs were captured by streptavidin-coated binding beads. After extensive wash, the captured DNAs were amplified and indexed with Illumina-indexing primers. Postcaptured DNA libraries were validated using Agilent TapeStation (Agilent) and quantified using Qubit 2.0 Fluorometer and Real-Time PCR (KAPA Biosystems). The sequencing libraries were multiplexed and clustered onto a lane of a flowcell. After clustering, the flowcell was loaded onto the Illumina HiSeq instrument according to the manufacturer's instructions. The samples were sequenced using a 2×150 bp Paired End configuration. Image analysis and base calling were conducted by the HiSeq Control Software. Raw sequence data (.bcl files) generated from Illumina HiSeq were converted into fastq files and demultiplexed using Illumina bcl2fastq 2.17 software. One mismatch was allowed for index sequence identification.

Sequence alignment, estimation and removal of mouse reads, and variant calling

Using the mouse contamination estimation method described previously by Jo and colleagues (6), we observed that estimated mouse contamination was very low (0.0%–1.4%), with the exception of one sample, CHP149R, for which the estimated mouse contamination was 24.3%. To remove potential mouse contaminating reads, we aligned to a concatenated human (hg38) and mouse (mm39) reference genome and removed reads aligning to the mouse genome, an approach that has been previously benchmarked as an effective method for high-quality human variant calling (6, 7). Alignment to this hybrid reference from the 2×150 bp sequencing configuration was performed using bwa v0.7.17 with default parameters (8), and bam files were merged and indexed using samtools v1.6 (9). Human reads were extracted using a script modified from Jo and colleagues (6), and calculation of depth of coverage was performed using mosdepth v0.3.1 (10).

Variant calling for single-nucleotide variants (SNV) and small indels was performed using Mutect2 in gatk v4.2.0.0 (11) with the gnomAD germline resource, 1,000 genome panels of normals, and default parameters for tumor-only mode. Variant annotation was performed using Annovar v2020–06–08 using exac03 (12), avsnp147 (13), and cosmic70 (14) databases. The Matched Annotation from NCBI and EMBL-EBI (MANE) canonical transcript was used for amino acid alteration annotation when available. Copy-number variants (CNV) were called from the human-specific bam files using CNVkit v0.9.9 (15) with the default circular binary segmentation strategy (16), and the genome-wide heat map was generated with the de-emphasize color scheme. Downstream analysis and plotting was performed using R v4.0.4 (17) and ggplot2 (18).

Data availability

The data generated in this study are publicly available in dbGaP with the accession number phs002323.v2.p1.

Statistical analyses

Statistical analysis was performed using R v4.0.4 (17). Pairwise statistical comparisons were assessed using the two-sided Welch's *t* test, and multiple testing correction was performed using Bonferroni correction with *P* values as noted in figure legends. Power analysis was performed using the function "power.t.test" with a significance level of 0.05 and power of 0.80.

Results

Identification and expansion of leukemic cells from paired preinfusion and relapse time points

We identified 13 patients with B-ALL who were treated with anti-CD19 CAR T-cell therapy and subsequently relapsed (**Fig. 1A**; Supplementary Table S1). The patients were all children and young adults (eight female and five male; age range, 5–21; median age, 10). Eight developed CD19$^-$ relapse after therapy, and five developed CD19$^+$ relapse. For all 13 patients, we acquired leukemic cells from both the pre-treatment and relapse time points. One patient (CHP105) had a prior CAR T-cell infusion and developed CD19$^+$ relapse, and subsequently relapsed with CD19$^-$ disease after a second CAR T-cell infusion. For this patient, the paired preinfusion and relapse samples represented the leukemic cells after the first infusion and before the second infusion (CHP105R) and the CD19$^-$ relapse after the second infusion (CHP105R2). Of these 26 total samples, six were previously studied by Sotillo and colleagues (3): CHP101/CHP101R, CHP105R/105R2, CHP107R, and CHP133R.

To achieve adequate cell counts for deep WES, B-ALL cells were expanded in a mouse PDX model. PDX mouse spleens were harvested, and cells were sorted to negatively select for mouse CD45 and positively select for human CD45 or human CD19 (Supplementary Fig. S1A). WES was performed on the sorted human leukemic cells. The mean read depth across exome regions was 471.4X (range, 359.8X–789.7X), with the highest depth in CHP149R, which underwent two rounds of sequencing to ensure adequate coverage (Supplementary Fig. S1B and S1C).

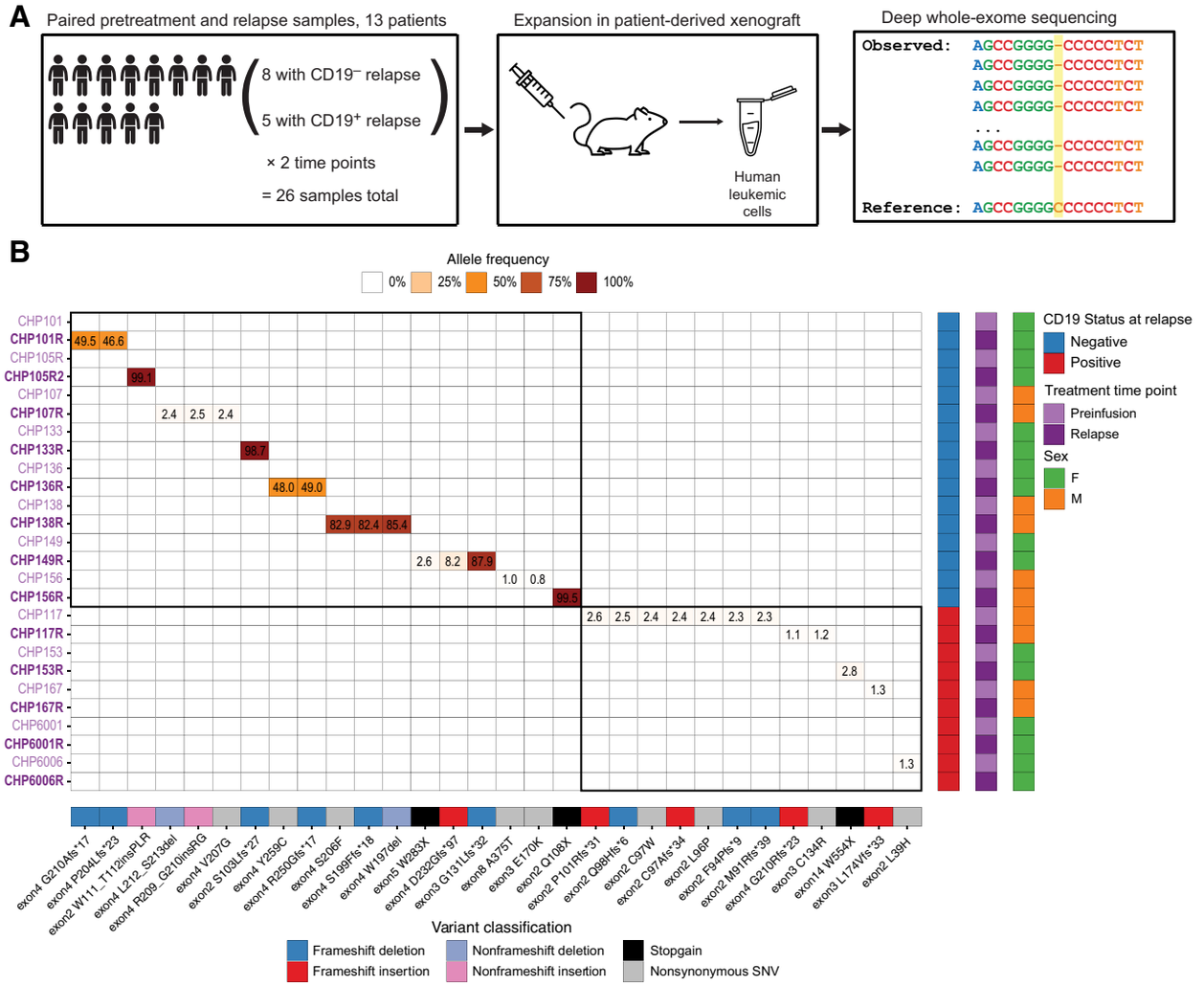

Figure 1.

Identification of relapse-specific *CD19* SNVs and small indels in leukemic cells using deep WES. **A,** Experimental strategy for identifying relapse-specific mutations. Paired preinfusion and relapse samples were identified from 13 children and young adults with B-ALL treated with CD19-targeted CAR T-cell therapy. Eight of the patients subsequently had a CD19$^-$ relapse, and five of the patients subsequently had a CD19$^+$ relapse. Leukemic cells from each of these 26 patient time points were expanded in a mouse patient-derived xenograft model, and DNA from sorted human cells underwent deep WES in one independent experiment. **B,** Heat map showing SNV and small indels identified from deep WES. Each row represents a patient time point, with paired pretreatment (light purple) and relapse (dark purple) time points listed in sequence. The eight patients who relapsed with CD19$^-$ leukemic cells are listed first (top-left box), followed by the five patients who relapsed with CD19$^+$ leukemic cells (bottom-right box). Columns represent SNVs and small indels, annotated by protein-coding changes (bottom bar). Each cell of the heat map is shaded by allele frequency, with numerical values, indicating cells for which allele frequency was detectable (>0%).

Deep WES reveals somatic *CD19* mutations specific to CD19$^-$ relapses

We identified 30 nonsynonymous SNVs and small indels in the *CD19* coding region across samples (**Fig. 1B**; Supplementary Table S2). Owing to the depth of sequencing, subclonal variants with allele frequencies as low as 0.8% were detectable. Among the eight patients with CD19$^-$ relapse, seven were observed to harbor nonsynonymous *CD19* variants with approximately heterozygous mutant allele frequencies or higher (>45%) at the relapse time point that were not detected at the preinfusion time point (**Fig. 1B**, top-left box). Patient CHP107 was the only case of CD19$^-$ relapse without a high-frequency *CD19* mutation at the relapse time point; this patient has previously been shown to be a case of unintentional CAR introduction into a leukemic B-cell that led to masking of the CD19 epitope (19). In contrast, none of five patients with CD19$^+$ relapse were observed to harbor nonsynonymous *CD19* variants above allele frequencies of 3% in the preinfusion or relapse time points (**Fig. 1B**, bottom-right box).

Examination of the *CD19* variants detected at CD19$^-$ relapse suggests alterations likely to be deleterious to the CD19 protein. CHP101R was observed to harbor two frameshift deletions in exon 4 with 49.5% and 46.6% allele frequencies, suggestive of two separate heterozygous mutations. Likewise, CHP136R was observed to harbor a nonsynonymous SNV with 48.0% allele frequency and a frameshift deletion in exon 4 with 49.0% allele frequency, suggestive of two

heterozygous mutations. Mutations in exon 2 with >98% allele frequency were observed in CHP105R2, CHP133R, and CHP156R that were classified as a non-frameshift insertion, frameshift deletion, and stop-gain, respectively. CHP138R was observed to harbor a nonsynonymous SNV, frameshift deletion, and nonframeshift deletion at allele frequencies in the range of 82.4% to 85.4%, suggestive of dominant subclonal mutations. CHP149R was observed to harbor a frameshift deletion in exon 3 at 87.9%, a frameshift insertion in exon 4 at 8.2%, and a stop-gain in exon 5 at 2.6%, suggestive of subclonal mutations with the prominent frameshift deletion in exon 3. None of these mutations were detectable in the preinfusion time points, and the only preinfusion *CD19* variants observed among the patients with subsequent CD19$^-$ relapse were two nonsynonymous SNVs in CHP156 at ≤1% allele frequency. Genes associated with B-cell markers other than *CD19* did not demonstrate a pattern of relapse-specific mutations (Supplementary Fig. S2A). In summary, among the eight CD19$^-$ patient samples, our data confirmed the presence of relapse-specific *CD19* mutations in three patient time points that overlapped with Sotillo and colleagues (ref. 3; CHP101R, CHP105R2, and CHP133R), as well as in the additional patients CHP136R, CHP138R, CHP149R, and CHP156R, whereas this trend was not observed in the five CD19$^+$ patient samples or in other B-cell genes.

CHP101R and CHP136R represented cases in which two nonsynonymous variants emerged with approximately 50% allele frequency. We asked whether these variants likely occurred on separate parental chromosomes, which would explain a "two-hit" inactivation of both copies of *CD19*. To this end, we assessed the phase of these variants to evaluate whether they existed in *cis* (on the same parental chromosome) or in *trans* (on separate parental chromosomes). Although phasing of somatic variants is generally challenging with short-read sequencing data, we noted that the variants in both patients were within approximately 20–30 base pairs, allowing us to directly assess variant phase by filtering to the reads that cover both genomic coordinates (9, 20). For CHP101R, reads covering both variant positions suggested variants in *trans*: Among the 520 reads covering both positions, 484/520 (∼93%) supported *trans* positioning, 0/520 (0%) supported *cis* positioning, 31/520 (∼6%) were the reference genome, and 5/520 (<1%) were another variant (Supplementary Fig. S3A and S3B). Similarly, for CHP136R, the vast majority of reads (613/634, ∼97%) supported *trans* positioning, 0/634 (0%) supported *cis* positioning, 15/634 (∼2%) were the reference genome, and the rest (<1%) were other variants (Supplementary Fig. S4A and S4B). Histograms of variant allele frequencies in these and most other samples displayed peaks at 0%, 50%, and 100%, pointing away from the concept of extensive and complex tumor clonality (Supplementary Fig. S5). These results are supportive of a dominant leukemic clone in these two patients harboring one heterozygous *CD19* variant on each parental chromosome, inactivating both copies of *CD19* in each cell for these two patients.

CNV analysis reveals preexisting and relapse-specific *CD19* deletions

We used CNVkit (15) to estimate CNVs in all samples (Supplementary Fig. S6). By filtering to CNVs with absolute $\log_2$ copy-number ratio greater than 0.75, we identified deletions in the *CD19* gene region in five of the eight patients with CD19$^-$ relapse (**Fig. 2A**, top-left box). *CD19* deletions were relapse-specific for CHP105R2, CHP138R, CHP149R, and CHP156R, and a *CD19* deletion was present in CHP133 at the preinfusion time point. All five of these patients were observed to harbor SNVs or small indels in *CD19* at allele frequencies >80% (**Fig. 1B**), supportive of a mechanism of deletion of *CD19* on one parental chromosome and one or more SNVs or small indels affecting the other chromosome. None of the five patients with CD19$^+$ relapse were found to harbor *CD19* deletions at the preinfusion or relapse time points, and recurrent copy-number events were not consistently observed in genes associated with the B-cell markers CD20 (*MS4A1*), CD22, CD34, CD38, or PAX5 (**Fig. 2A**).

Higher pretreatment mutational burden nonsignificantly associates with CD19$^-$ relapse

We asked whether the mutational burden of the leukemic cells at the preinfusion time point associated with subsequent development of CD19$^-$ relapse. Mutational burden in solid tumors has been shown to associate with higher response rates to immune checkpoint inhibitor (ICI) therapy, likely owing to tumor-specific neoantigen presentation and increased TCR-mediated T-cell cytotoxicity (21, 22). The association between mutational burden and therapy modalities other than ICIs is uncertain and likely to be dependent on treatment context, with higher mutational burden being associated with worse prognosis in non–ICI treated patients (23). In the case of CAR T-cell therapy directed toward CD19, a reasonable hypothesis is that higher mutational burden may be associated with an increased probability of harboring a subclonal *CD19* mutation that can expand under selective pressure to result in CD19$^-$ relapse. To assess this hypothesis, we estimated mutational burden from our WES by assessing (1) the total number of SNVs and small indels, (2) the percentage of the genome with a CNV, and (3) variants in genes associated with genome instability and hypermutation. The total number of SNVs and small indels was sensitive to variant filtering strategies, with a mean of 30,542 and 11,774 variants per sample called without filtering and with the most stringent criteria (Supplementary Fig. S7A), respectively. Across variant filtering criteria, the eight patients who had CD19$^-$ status at relapse had relatively higher numbers of variants detected at the preinfusion time point compared with the five patients who had CD19$^+$ status at relapse, although these results were not statistically significant (Supplementary Fig. S7B, $P = 0.058$–0.11). Power analysis suggested that approximately 17 patients per relapse group would be required to achieve a statistically significant result at an alpha level of 0.05 with 80% power. There was no significant difference in mutational burden in the pretreatment versus relapse time points in the CD19$^-$ group, and there was a nonsignificant increase in mutational burden between pretreatment and relapse time points in the CD19$^+$ relapse group (Bonferroni adjusted $P = 0.062$, unadjusted $P = 0.015$). Comparison of CD19$^-$ and CD19$^+$ showed no significant difference between mutational burden at either the pretreatment or relapse time points (Supplementary Fig. S7C).

The percentage of genome with aberrant copy number has been used as a global marker of genomic instability (24), with potential relevance to CD19$^-$ relapse through the possibility that cancers with unstable genomes may be more likely to acquire relapse-enabling mutations. Indeed, we found that CHP133, the only patient that harbored a preexisting *CD19* deletion before CAR T-cell infusion, had evidence of extensive genomic instability, with over 30% of the genome estimated to harbor an aberrant copy number in the preinfusion and relapse time points with an absolute $\log_2$ cutoff value of 0.75 (Supplementary Fig. S8A). This level of genome instability was not seen in the remaining samples, and the percentage of the genome with a CNV at the preinfusion time point was not significantly predictive of subsequent CD19$^-$ relapse across patients (Supplementary Fig. S8B).

Finally, we investigated whether mutations in genes associated with genome instability and hypermutation were overrepresented in the pretreatment leukemic cells for patients with subsequent CD19$^-$

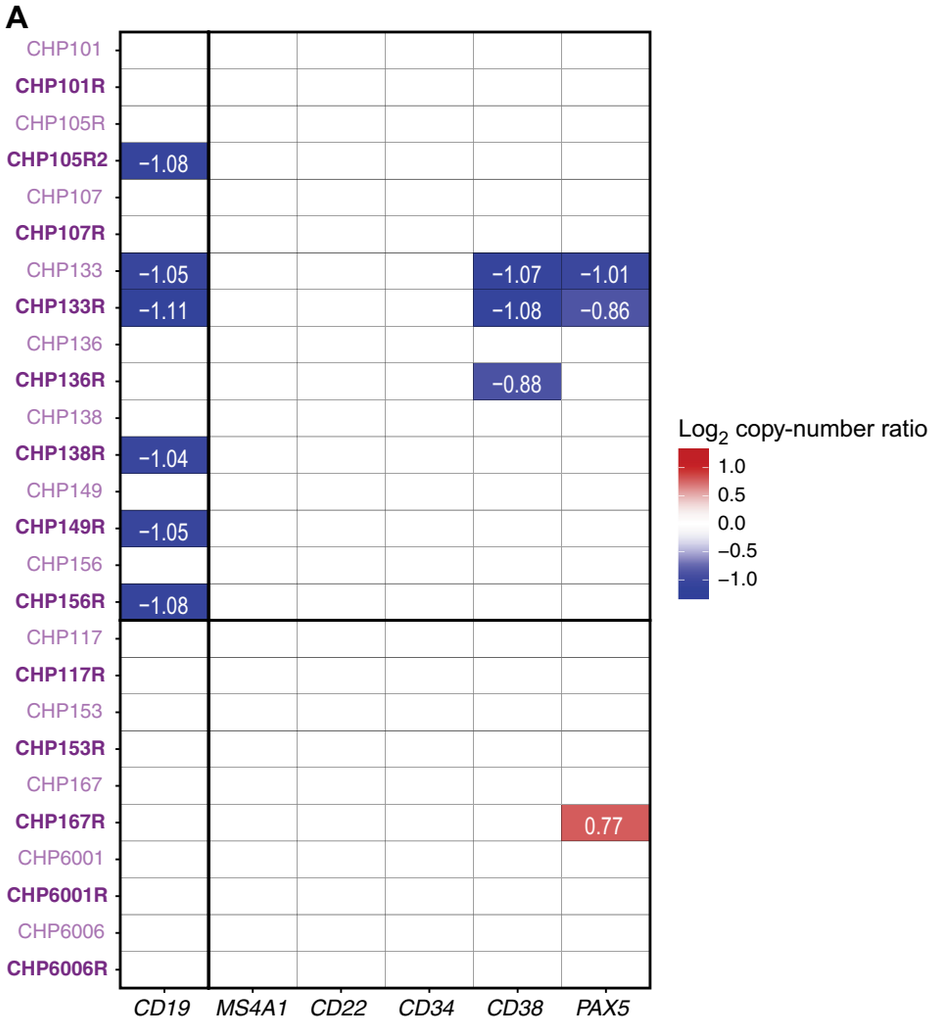

Figure 2.

Identification of relapse-specific and preexisting copy-number variants involving *CD19* and other B-cell genes using deep whole-exome sequencing. **A,** Heat map showing copy-number CNV in *CD19* and other B-cell genes. Shown are the CNVs called by CNVkit that passed an absolute $\log_2$ fold-change threshold of 0.75. Rows represent patient time point, with paired pretreatment (light purple) and relapse (dark purple) time points listed in sequence. The eight patients who relapsed with CD19$^-$ leukemic cells are listed first (top-left and top-right boxes), followed by the five patients who relapsed with CD19$^+$ leukemic cells (bottom-left and bottom-right boxes). Columns indicate genes associated with B-cell markers: *CD19*, *MS4A1* (encoding CD20), *CD22*, *CD34*, *CD38*, and *PAX5*.

relapse. We called variants in *TP53*, *POLE*, *POLD1*, and *SETD2*, genes associated with genomic instability and hypermutation (refs. 25–27; Supplementary Table S2; Supplementary Fig. S9). 3/8 of the patients with CD19$^-$ relapse had an observed mutation in one of these genes with at least approximately heterozygous allele frequency (>45%): CHP101R, CHP136/CHP136R, and CHP138, whereas 0/5 of the patients with CD19$^+$ relapse had an observed variant in one of these genes with allele frequency >6%. These variants suggest that mutations in genome instability genes may play a role in CD19$^-$ relapse, although limited sample size may have restricted the generalizability of this observation.

Discussion

The remarkable response rates of anti-CD19 CAR T-cell therapy in pediatric B-ALL are a testament to the clinical potential of this therapeutic modality, yet antigen escape through emergence of CD19$^-$ leukemic clones is a major mechanism of relapse. By using deep WES on leukemic populations at treatment and CD19$^+$ or CD19$^-$ relapse, we observed the emergence of likely deleterious coding variants at heterozygous or homozygous allele frequencies that associated with CD19$^-$ relapse populations compared with preinfusion leukemic cells or CD19$^+$ relapse populations. The depth of sequencing allowed us to identify CD19 variants with allele frequency as low as 0.8%, yet none of the variants observed in the CD19$^-$ relapse time points were detected at the preinfusion time points, suggesting that they were likely present at very rare frequencies or emerged during the course of therapy.

The identification of predictive biomarkers of CD19$^-$ relapse subsequent to anti-CD19 CAR T-cell therapy remains an intriguing and important question. Pillai and colleagues (28) reported that preinfusion dim CD19 expression and rare CD19$^-$ events by flow cytometry were not predictive of response or relapse to anti-CD19 CAR T-cell therapy. In our cohort, we observed one preexisting *CD19* genomic variant, a *CD19* deletion in CHP133, which likely represented a first hit that allowed a relapse-specific frameshift mutation in the other *CD19* allele to lead to CD19$^-$ relapse in this patient. This represents an intriguing example in which genome-wide copy-number instability, which included a deletion in one parental copy of *CD19* before therapy, likely predisposed this patient to CD19$^-$ relapse due to the need for only one more mutation in the remaining *CD19* allele. In our cohort, the preexisting genomic instability in CHP133 appeared to be an exceptional case.

Despite our deep sequencing, preexisting *CD19* variants were not observed in the remaining patients, and preinfusion mutational

burden at the level of SNVs and small indels and CNVs were not significantly associated with subsequent CD19$^-$ relapse. Furthermore, SNVs and small indels that were detected at baseline did not necessarily foreshadow subsequent CD19$^-$ relapse. Among the patients with CD19$^-$ relapse, the only one with a detected preexisting SNV or small indel in *CD19* was CHP156, for which two nonsynonymous SNVs at 0.8%–1.0% were detected at baseline but not at relapse. Among the patients with CD19$^+$ relapse, three had a detected preexisting SNV or small indel in *CD19*—CHP117, CHP167, and CHP6006—of which, these variants were not detected at the relapse time points. In particular, CHP117 had seven detected variants at 2.3%–2.6%, including frameshift insertions and deletions, that were observed at the pretreatment time point but not observed at the CD19$^+$ relapse time point. Whether these represent a single hypermutated clone or variants in separate clones is unclear, and the lack of selection toward one or more of these variants suggests an alternate mechanism of relapse for this patient.

With the exception of the preexisting *CD19* deletion in CHP133, the timing of relapse-associated *CD19* variants remains unanswered. Whereas conventional next-generation sequencing is limited for ultra-rare mutation detection due to a technical error of approximately 0.1%, technologies, such as droplet digital PCR and Duplex Sequencing, may provide a strategy for detection of preexisting mutations with lower error rates (29, 30). Methods such as single-cell DNA sequencing may provide a strategy to better delineate clonal evolution, although low per-cell target coverage may limit detection of *CD19* variants (31). Further studies with larger patient sample sizes will be important to help clarify the possible role of preexisting mutations and mutational burden as a predictive therapeutic marker.

A limitation of our study is the use of PDX expansion to obtain a sufficiently high quantity of DNA for analysis. Although some studies report that human leukemic cells can recapitulate the clonal composition in a PDX model, particularly with respect to driver genes (32, 33), others have shown that PDX models are initially highly polyclonal and serial transplantation decreases the number of clones (34). Variant allele frequencies that we observed in the PDX-expanded cells likely correlate with the true frequencies in the original human sample, particularly for variants with high true allele frequency, but we cannot exclude the possibility of biases or variation affecting our observed allele frequency values. Majzner and Mackall (35) highlight open areas of investigation in CAR T-cell antigen escape in cancers beyond pediatric B-ALL. Limited data from post-CAR relapses in adult B-ALL suggest that CD19$^-$ relapses may be relatively rare (<10% of complete responses), and there is paucity of clinical data investigating cell surface CD19 expression from patients with non-Hodgkin's lymphoma. In addition, CD22 antigen escape appears to occur due to diminished expression in CD22 through a nongenomic mechanism (35). A study of 28 patients with diffuse large B-cell lymphoma reports that preexisting *CD19* mutations or reduced CD19 expressions are relatively uncommon and not associated with poor outcome to CAR T-cell therapy (36), although further studies with paired pretreatment and relapse time points will be necessary to better understand the possible role of CD19 antigen escape in lymphoma.

Authors' Disclosures

G.M. Chen reports grants from Canadian Institutes of Health Research during the conduct of the study. S.A. Grupp reports grants and personal fees from Novartis during the conduct of the study as well as a patent for CAR T toxicity management issued, licensed, and with royalties paid from Novartis; study support from Kite, Vertex, and Servier; consulting for Roche, GSK, AmerisourceBergen, CBMG, Eureka, and Janssen/JnJ; and is on study steering committees or scientific advisory boards for Jazz, Adaptimmune, TCR2, Cellectis, Juno, Vertex, Allogene and Cabaletta. K. Tan reports grants from NIH during the conduct of the study. No disclosures were reported by the other authors.

Authors' Contributions

G.M. Chen: Conceptualization, resources, software, formal analysis, supervision, funding acquisition, investigation, methodology, writing–original draft, project administration, writing–review and editing. **C.-H. Chen:** Software, formal analysis, investigation, methodology, writing–original draft, writing–review and editing. **J. Perazzelli:** Resources, investigation, methodology. **S.A. Grupp:** Conceptualization, resources, supervision, funding acquisition, investigation, methodology, writing–review and editing. **D.M. Barrett:** Conceptualization, resources, supervision, funding acquisition, investigation, methodology, writing–review and editing. **K. Tan:** Conceptualization, resources, formal analysis, supervision, funding acquisition, investigation, writing–original draft, project administration, writing–review and editing.

Acknowledgments

We thank the Children's Hospital of Philadelphia Flow Cytometry Core for their assistance with cell sorting, and the Research Information Services for providing computing support. This work was supported by National Institutes of Health of United States of America grants CA232361 (to D.M. Barrett and S.A. Grupp) and CA233285 (to K. Tan), a Doris Duke Charitable Foundation Clinical Scientist Development Award and a Stand Up To Cancer Innovative Research grant, grant number SU2C-AACR-IRG 12–17 (to D.M. Barrett), a CIHR Doctoral Foreign Study Award #433117 (to G.M. Chen). Stand Up To Cancer (SU2C) is a division of the Entertainment Industry Foundation. The indicated SU2C research grant is administered by the American Association for Cancer Research, a scientific partner of SU2C.

Note

Supplementary data for this article are available at Cancer Immunology Research Online (http://cancerimmunolres.aacrjournals.org/).

Received March 8, 2022; revised July 27, 2022; accepted October 12, 2022; published first October 18, 2022.

References

1. Maude SL, Laetsch TW, Buechner J, Rives S, Boyer M, Bittencourt H, et al. Tisagenlecleucel in children and young adults with B-cell lymphoblastic leukemia. N Engl J Med 2018;378:439–48.
2. Grupp SA, Kalos M, Barrett D, Aplenc R, Porter DL, Rheingold SR, et al. Chimeric antigen receptor–modified T cells for acute lymphoid leukemia. N Engl J Med 2013;368:1509–18.
3. Sotillo E, Barrett DM, Black KL, Bagashev A, Oldridge D, Wu G, et al. Convergence of acquired mutations and alternative splicing of CD19 enables resistance to CART-19 immunotherapy. Cancer Discov 2015;5:1282–95.
4. Orlando EJ, Han X, Tribouley C, Wood PA, Leary RJ, Riester M, et al. Genetic mechanisms of target antigen loss in CAR19 therapy of acute lymphoblastic leukemia. Nat Med 2018;24:1504–6.
5. Barrett DM, Seif AE, Carpenito C, Teachey DT, Fish JD, June CH, et al. Noninvasive bioluminescent imaging of primary patient acute lymphoblastic leukemia: a strategy for preclinical modeling. Blood 2011;118:e112–7.
6. Jo S-Y, Kim E, Kim S. Impact of mouse contamination in genomic profiling of patient-derived models and best practice for robust analysis. Genome Biol 2019;20:231.
7. Rokita JL, Rathi KS, Cardenas MF, Upton KA, Jayaseelan J, Cross KL, et al. Genomic profiling of childhood tumor patient-derived xenograft models to enable rational clinical trial design. Cell Rep 2019;29:1675–89.
8. Li H, Durbin R. Fast and accurate short read alignment with burrows-wheeler transform. Bioinformatics 2009;25:1754–60.
9. Li H, Handsaker B, Wysoker A, Fennell T, Ruan J, Homer N, et al. The sequence alignment/map format and SAMtools. Bioinformatics 2009;25:2078–9.

10. Pedersen BS, Quinlan AR. Mosdepth: quick coverage calculation for genomes and exomes. Bioinformatics 2018;34:867–8.
11. Auwera VAG, O'Connor BD. Genomics in the Cloud: using Docker, GATK, and WDL in Terra. 1st ed. Sebastopol, CA: O'Reilly Media; 2020.
12. Lek M, Exome Aggregation Consortium, Karczewski KJ, Minikel EV, Samocha KE, Banks E, et al. Analysis of protein-coding genetic variation in 60,706 humans. Nature 2016;536:285–91.
13. Sherry ST, Ward MH, Kholodov M, Baker J, Phan L, Smigielski EM, et al. dbSNP: the NCBI database of genetic variation. Nucleic Acids Res 2001;29: 308–11.
14. Forbes SA, Beare D, Gunasekaran P, Leung K, Bindal N, Boutselakis H, et al. COSMIC: exploring the world's knowledge of somatic mutations in human cancer. Nucleic Acids Res 2015;43:D805–11.
15. Talevich E, Shain AH, Botton T, Bastian BC. CNVkit: genome-wide copy-number detection and visualization from targeted DNA sequencing. PLoS Comput Biol; 2016;12:e1004873.
16. Venkatraman ES, Olshen AB. A faster circular binary segmentation algorithm for the analysis of array CGH data. Bioinformatics; 2007;23:657–63.
17. Ihaka R, Gentleman R. R: a language for data analysis and graphics. J Comput Graph Stat 1996;5:299–314.
18. Wickham H. Ggplot2: elegant graphics for data analysis. New York, NY: Springer; 2009.
19. Ruella M, Xu J, Barrett DM, Fraietta JA, Reich TJ, Ambrose DE, et al. Induction of resistance to chimeric antigen receptor T-cell therapy by transduction of a single leukemic B cell. Nat Med 2018;24:1499–503.
20. Thorvaldsdóttir H, Robinson JT, Mesirov JP. Integrative genomics viewer (IGV): high-performance genomics data visualization and exploration. Brief Bioinform 2013;14:178–92.
21. Goodman AM, Kato S, Bazhenova L, Patel SP, Frampton GM, Miller V, et al. Tumor mutational burden as an independent predictor of response to immunotherapy in diverse cancers. Mol Cancer Ther 2017;16:2598–608.
22. Sha D, Jin Z, Budczies J, Kluck K, Stenzinger A, Sinicrope FA. Tumor mutational burden as a predictive biomarker in solid tumors. Cancer Discov 2020;10:1808–25.
23. Valero C, Lee M, Hoen D, Wang J, Nadeem Z, Patel N, et al. The association between tumor mutational burden and prognosis is dependent on treatment context. Nat Genet 2021;53:11–5.
24. Lalonde E, Ishkanian AS, Sykes J, Fraser M, Ross-Adams H, Erho N, et al. Tumour genomic and microenvironmental heterogeneity for integrated prediction of 5-year biochemical recurrence of prostate cancer: a retrospective cohort study. Lancet Oncol 2014;15:1521–32.
25. Wang F, Zhao Q, Wang Y-N, Jin Y, He M-M, Liu Z-X, et al. Evaluation of POLE and POLD1 mutations as biomarkers for immunotherapy outcomes across multiple cancer types. JAMA Oncol 2019;5:1504–6.
26. Pfister SX, Ahrabi S, Zalmas L-P, Sarkar S, Aymard F, Bachrati CZ, et al. SETD2-dependent histone H3K36 trimethylation is required for homologous recombination repair and genome stability. Cell Rep 2014;7:2006–18.
27. Negrini S, Gorgoulis VG, Halazonetis TD. Genomic instability—an evolving hallmark of cancer. Nat Rev Mol Cell Biol 2010;11:220–8.
28. Pillai V, Muralidharan K, Meng W, Bagashev A, Oldridge DA, Rosenthal J, et al. CAR T-cell therapy is effective for CD19-dim B-lymphoblastic leukemia but is impacted by prior blinatumomab therapy. Blood Adv 2019;3:3539–49.
29. Hindson CM, Chevillet JR, Briggs HA, Gallichotte EN, Ruf IK, Hindson BJ, et al. Absolute quantification by droplet digital PCR versus analog real-time PCR. Nat Methods 2013;10:1003–5.
30. Kennedy SR, Schmitt MW, Fox EJ, Kohrn BF, Salk JJ, Ahn EH, et al. Detecting ultralow-frequency mutations by Duplex Sequencing. Nat Protoc 2014;9: 2586–606.
31. Navin N, Kendall J, Troge J, Andrews P, Rodgers L, McIndoo J, et al. Tumour evolution inferred by single-cell sequencing. Nature 2011;472:90–4.
32. Wang K, Sanchez-Martin M, Wang X, Knapp KM, Koche R, Vu L, et al. Patient-derived xenotransplants can recapitulate the genetic driver landscape of acute leukemias. Leukemia 2017;31:151–8.
33. Schmitz M, Breithaupt P, Scheidegger N, Cario G, Bonapace L, Meissner B, et al. Xenografts of highly resistant leukemia recapitulate the clonal composition of the leukemogenic compartment. Blood 2011;118:1854–64.
34. Belderbos ME, Koster T, Ausema B, Jacobs S, Sowdagar S, Zwart E, et al. Clonal selection and asymmetric distribution of human leukemia in murine xenografts revealed by cellular barcoding. Blood 2017;129:3210–20.
35. Majzner RG, Mackall CL. Tumor antigen escape from CAR T-cell therapy. Cancer Discov 2018;8:1219–26.
36. Jain MD, Zicchedda B, Coughlin CA, Faramand R, Griswold AJ, Reid KM, et al. Genomic drivers of large B-cell lymphoma resistance to CD19 CAR-T therapy. Blood 2021;138:42–42.